IEEE CSS

Received 20 February 2023; revised 19 May 2023; accepted 8 June 2023. Date of publication 26 June 2023;
date of current version 14 July 2023. Recommended by Senior Editor Prof. Lacra Pavel.

Digital Object Identifier 10.1109/OJCSYS.2023.3289771

Closed-Loop Kinematic and Indirect Force Control of a Cable-Driven Knee Exoskeleton: A Lyapunov-Based Switched Systems Approach

CHEN-HAO CHANG, JONATHAN CASAS, AND VICTOR H. DUENAS (Member, IEEE)

Department of Mechanical and Aerospace Engineering, Syracuse University, Syracuse, NY 13244 USA

CORRESPONDING AUTHOR: VICTOR H. DUENAS (e-mail: vhduenas@syr.edu)

This work was supported in part by the Collaboration for Unprecedented Success and Excellence (CUSE) Grant Program at Syracuse University.

This work involved human subjects or animals in its research. Approval of all ethical and experimental procedures and protocols was granted by Syracuse University IRB under Application No. 19-355, and performed in line with 45 CFR 46 (the Common Rule).

ABSTRACT Lower-limb exoskeletons can aid restoring mobility in people with movement disorders. Cable-driven exoskeletons can offload their actuators away from the human body to reduce the weight imposed on the user and enable precise control of joints. However, ensuring limb coordination through bidirectional motion control of joints using cables raise the technical challenge of preventing the occurrence of undesired cable slackness or counteracting forces between cables. Thus, motivation exists to develop a control design framework that integrates both a joint control loop to ensure suitable limb tracking and a cable control loop to maintain cable tension properly. In this article, a two-layer control structure consisting of high and low-level controllers are developed to ensure a knee-joint exoskeleton system follows the desired joint trajectories and adjusts the cable tension, respectively. A repetitive learning controller is designed for the high-level knee joint tracking objective motivated by the periodic nature of the desired leg swings (i.e., to achieve knee flexion and extension). Low-level robust controllers are developed for a pair of cables, each actuated by an electric motor, to track target motor trajectories composed of motor kinematics and offset angles to mitigate cable slackness. The offset angles are computed using admittance models that exploit measurements of the cable tensions as inputs. Each electric motor switches its role between tracking the knee joint trajectory (i.e., the motor acts as the leader motor to achieve flexion or extension) and implementing the low-level controller (i.e., the motor acts as the follower motor to reduce slackness). Hence, at any time, one motor is the leader and the other is the follower. A Lyapunov-based stability analysis is developed for the high-level joint controller to ensure global asymptotic tracking and the low-level follower controller to guarantee global exponential tracking. The designed controllers are implemented during leg swing experiments in six able-bodied individuals while wearing the knee joint cable-driven exoskeleton. A comparison of the results obtained in two trials with and without using the admittance model (i.e., exploiting cable tension measurements) is presented. The experimental results indicate improved knee joint tracking performance, smaller control input magnitudes, and reduced cable slackness in the trial that leveraged cable tension feedback compared to the trial that did not exploit tension feedback.

INDEX TERMS Human-in-the-loop, lower-limb exoskeletons, Lyapunov methods, nonlinear control, switched systems.

I. INTRODUCTION

People with movement disorders following a neurological condition such as a spinal cord injury (SCI) experience limited range of motion, balance, mobility, and independence that diminish the quality of life [1], [2]. Lower-limb exoskeletons can assist people with SCI during rehabilitation and reduce the burden of physical therapists. Benefits of exoskeletal-assisted rehabilitation include restoring and improving gait function,

reducing the energetic costs of walking, and improving endurance [2]. Exoskeleton devices are equipped with actuators to provide limb assistance such as electrical motors [3], [4], [5], hydraulic [6] and pneumatic [7], [8] actuators. The selection of actuators is important since they increase the inertia of the exoskeleton potentially increasing the metabolic costs and inducing misalignment, which may lead to discomfort, pain, and even injury [9]. Cable-driven exoskeletons have been developed to reduce the weight and inertia of traditional rigid exoskeletons and provide precise joint control for limb assistance.

Cable-driven exoskeletons can offload the actuators away from the human body and provide torque at the joints using Bowden cables (that are connected to a separate actuation unit). Decoupling the actuators from the user can enable light-weight exoskeletons [10] for lower-limb [11], [12] and upper-limb [10], [13], [14] assistance. Cables cannot provide compressive forces; therefore, at least two cables are needed to achieve bi-directional motion control of one joint (agonist-antagonist movement) [15]. Thus, a constructive control design is motivated to ensure suitable coordination between cables to elicit smooth limb motion and avoid two major potential issues [16]: (1) cable slackness that can degrade the system's response time and control performance; and (2) counteracting cable forces being applied concurrently at the joint, which can lead to an unstable joint kinematic response and thus yield unnatural joint motion. This article develops a systematic layered control framework to mitigate the aforementioned issues and ensure knee joint tracking.

Solutions to prevent cable slackness are to pre-load and maintain cable tension using mechanical units such as compression springs in series with the Bowden cable sheath [17], pulling springs in series with the cable [18], and helical torsion springs [19]. Although these mechanical approaches can adjust cable tension, the system's response time increases (due to the spring's loading time) and its tension cannot be automatically controlled. Alternatively, designing control strategies can digitally adjust the cable tension by controlling the actuators directly (e.g., prescribe desired cable stiffness) to customize the interaction for different users. Force control has been widely implemented in upper-limb exoskeletons [20], [21], lower-limb exoskeletons [22], [23], [24], ankle actuators [25], exosuits [26], cycling [27], [28], and surgical manipulators [29]. Indirect force controllers exploit impedance or admittance-based models to generate desired trajectories based on kinematic and force inputs, respectively. This article exploits admittance models for the electric motors to adjust the tension of cables and thus mitigate slackness and counteracting forces in the knee exoskeleton.

Learning-based controllers are motivated for joint tracking since limb movements such as leg swings are repetitive or periodic. Repetitive control (RC) and iterative learning control (ILC) are two primary learning control methods for periodic tasks illustrated in applications such as upper-limb rehabilitation robots [30], lower-limb exoskeletons [31], functional electrical stimulation (FES)-cycling [27], and industrial robots [32], [33]. Learning control approaches seek to improve tracking performance by leveraging learned inputs from previous trials. ILC is usually implemented for discontinuous tasks in which the initial conditions are reset to the same values at the beginning of each trial [34]. Furthermore, ILC has been combined with model predictive control (MPC) [35] and reference-free learning MPC [36] to improve tracking performance. RC is implemented for continuous operation and the initial conditions are not reset [37]. Differently from our previous work in [38] that designs a robust controller to track the knee joint trajectory without experimental implementation, a repetitive learning controller is developed in this article leveraging the design in [37] to reduce the reliance on high-frequency and high-gain control.

In this article, a control framework segregated into a high-level joint controller and a low-level motor controller are designed, analyzed, and experimentally implemented using a cable-driven knee-joint exoskeleton. A pair of electric motors provide bi-directional motion about the knee joint. One motor is called the leader motor that implements the high-level input to track the desired joint kinematics (magnitude and direction). The complementary motor is called the follower motor that implements a low-level input to prevent undesired cable slackness and counteracting forces. When the desired direction of joint motion flips, the roles of the motors switch (i.e., the leader motor becomes the follower motor and vice versa). Compared to our previous work in [38], the main contributions in this article are as follows:

1) Low-level control inputs are designed using a robust control approach for the electric motors when each of them acts as the follower motor. The low-level controllers track the leader motor's angle and a kinematic offset term is generated using an admittance model, which exploits feedback of the tension of the cable (indirect force control) connected to the follower motor.
2) A repetitive learning controller is designed as a representative high-level controller to track periodic knee-joint trajectories and achieve leg swings while reducing the need for high gain and high-frequency feedback.
3) A Lyapunov-based stability analysis segregated into two theorems is developed to demonstrate that the novel designs of the high-level and low-level closed-loop controllers with input switching ensure global asymptotic and exponential tracking, respectively. The high-level and low-level control inputs, which leverage kinematic and cable force feedback, are shown to be bounded.
4) Experiments are conducted in six able-bodied individuals to demonstrate the performance of the low-level and high-level controllers. The results of two trials with (Controller A) and without (Controller B) using the admittance model (i.e., exploiting cable tension measurements as indirect force control) are discussed and compared.

The article is organized as follows. The dynamic models are introduced in Section II. In Section III, the repetitive learning controller is designed for the high-level control layer to

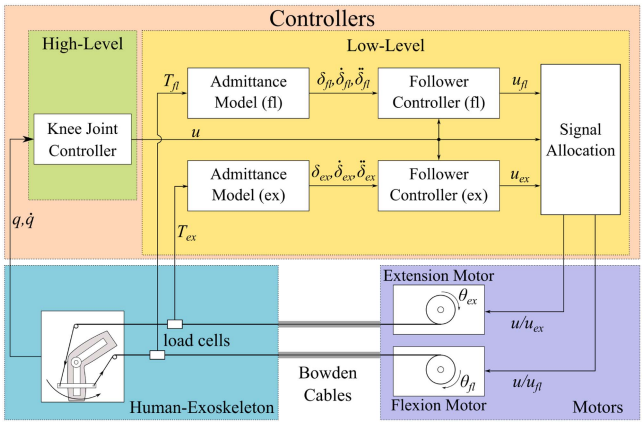

FIGURE 1. Schematic depicts the two-layer control system illustrated at the moment of achieving knee flexion as an example (see direction of the arrow in exoskeleton). The high-level knee joint controller exploits joint position q and velocity $\dot{q}$ to compute the control input u that is forwarded to the leader motor (e.g., in this example to the flexion motor). The admittance models with state variables $\delta_n, \dot{\delta}_n, \ddot{\delta}_n$ corresponding to extension and flexion motors, $n = \{ex, fl\}$ respectively, exploit cable tension feedback T_{ex}, T_{fl} to generate the target kinematic offset to compute the input into the follower motor. Thus, the high-level and low-level control inputs are allocated to the leader and follower motors, respectively, to achieve bi-directional motion (i.e., extension and flexion). The low-level control inputs for the extension and flexion motors are denoted as u_{ex}, u_{fl}, respectively. In this schematic, the high-level knee joint controller computes the knee flexion input u; thus, the flexion motor serves as the leader motor and the extension motor serves as the follower motor. To achieve knee extension, the roles of the leader and follower motors switch.

track a periodic knee joint trajectory. The designed low-level controllers for the electric motors and the admittance models are introduced in Section IV. The Lyapunov-based stability analyses for the high-level and low-level control loops are developed in Section V. Experimental results for controllers with and without the indirect force control are presented in Section VI, a discussion is presented in Section VII and the conclusion is presented in Section VIII.

II. DYNAMIC MODELS

A. CABLE-DRIVEN ACTUATOR SYSTEM

The lower-limb exoskeleton applies torque about the knee joint and is actuated by electric motors using customized cable-driven mechanisms (i.e., forces are transmitted via Bowden cables). A pair of electric motors is used to achieve knee joint extension (ex) and flexion (fl). To ensure smooth coordination between the pair of motors, the following roles are defined for each motor at any given time

1) The *leader* motor is the driving motor controlling the knee joint kinematics to achieve the desired knee joint angle and direction (i.e., flexion or extension).
2) The *follower* motor is the complementary motor seeking to mitigate cable slackness and prevent undesired counteracting forces with the leader motor.

A control framework inspired in our previous theoretical work in [38] is developed to design a high-level controller to track the desired knee joint trajectory and low-level controllers to mitigate cable slackness. The relationships between the designed high-level and low-level controllers with the roles of the motors at any given time are described as follows:

1) The *high-level* controller generates the control input to track the knee joint trajectory that is forwarded to the *leader* motor.
2) The *low-level* controllers generate control inputs for the pair of motors to avoid cable slackness and undesired counteracting forces when the role of each motor is assigned as the *follower* motor.
3) The control input for each motor switches between the *high-level* controller and its *low-level* controller depending if the motor is the *leader* or *follower*, respectively. Thus, at any given time, one motor is the *leader* and the second motor is the *follower*.
4) The low-level controller for a given motor is called *active* if the control input is fed into the motor (i.e., follower role). The low-level controller is called *inactive* if the control input is not being fed into the motor (i.e., motor has the leader role).

A schematic of the two-layer control system is presented in Fig. 1 , where the knee joint control input is denoted by u (high-level control input), and the follower motor control inputs for the extension and flexion motors are denoted by u_{ex}, u_{fl} (low-level control inputs), respectively.

B. KNEE-SHANK AND POWERED EXOSKELETON DYNAMIC MODEL

The knee-joint shank dynamics and the powered exoskeleton can be modeled as [39]

$$M(q)\ddot{q} + G(q) + P(q, \dot{q}) = \tau_e(t), \tag{1}$$

where $q : \mathbb{R}_{\geq t_0} \to \mathbb{R}$, $\dot{q} : \mathbb{R}_{\geq t_0} \to \mathbb{R}$, and $\ddot{q} : \mathbb{R}_{\geq t_0} \to \mathbb{R}$ are the measurable knee joint angle, measurable joint angular velocity, and unmeasurable angular acceleration, $t_0 \in \mathbb{R}_{\geq 0}$ denotes the initial time. The inertia of the combined knee-shank and exoskeleton is denoted as $M : \mathbb{R} \to \mathbb{R}_{>0}$; $G : \mathbb{R} \to \mathbb{R}$ denotes the gravitational effects; $P : \mathbb{R} \times \mathbb{R} \to \mathbb{R}$ denotes the passive viscoelastic and damping effects. The torque applied by the leader motor is denoted as $\tau_e : \mathbb{R}_{\geq t_0} \to \mathbb{R}$, and can be defined as

$$\tau_e(q, \dot{q}, t) \triangleq B_e(t)u(q, \dot{q}, t), \tag{2}$$

where $B_e : \mathbb{R}_{\geq t_0} \to \mathbb{R}_{>0}$ is the control effectiveness of the leader motor at time t, and is defined as

$$B_e(t) \triangleq \begin{cases} B_{fl} & \text{if } \operatorname{sgn}(u) \geq 0 \\ B_{ex} & \text{if } \operatorname{sgn}(u) < 0 \end{cases}, \tag{3}$$

where $B_{fl}, B_{ex} \in \mathbb{R}_{>0}$ are the control effectiveness values of the flexion and extension motor, respectively. The signum function $\operatorname{sgn}(\cdot) = 1$ for $(\cdot) > 0$, $\operatorname{sgn}(\cdot) = 0$ for $(\cdot) = 0$, and $\operatorname{sgn}(\cdot) = -1$ for $(\cdot) < 0$. The high-level knee joint control input $u : \mathbb{R}_{\geq t_0} \to \mathbb{R}$ is designed in Section III.

C. FOLLOWER MOTOR DYNAMIC MODEL

The follower motor system dynamics can be modeled as follows

$$J_n\ddot{\theta}_n + D_n\dot{\theta}_n + d_n(t) = B_n u_n(t), \forall n, \tag{4}$$

where $n = \{ex, fl\}$ is the index corresponding to the extension and flexion motor, $\theta_n, \dot{\theta}_n, \ddot{\theta}_n : \mathbb{R}_{\geq t_0} \to \mathbb{R}$ denote the motor's measurable angular position, velocity, and unmeasurable acceleration. The inertia of the motor is denoted by $J_n \in \mathbb{R}_{>0}$, the damping coefficient is denoted by $D_n \in \mathbb{R}$, an additive disturbance is denoted by $d_n : \mathbb{R}_{\geq t_0} \to \mathbb{R}$, and the input effectiveness for each motor is denoted as $B_n \in \mathbb{R}_{>0}$, $\forall n$. The assigned low-level follower control input is denoted as $u_n : \mathbb{R}_{\geq t_0} \to \mathbb{R}$, $\forall n$ and designed in Section IV.

The following properties and assumptions for (1) and (4) are exploited in the subsequent control design and stability analysis.

Property 1: $c_m \leq M(q) \leq c_M$, where $c_m, c_M \in \mathbb{R}_{>0}$ are known constants [40].

Property 2: The inverse M^{-1} is bounded as $\frac{1}{c_M} \leq M^{-1}(q) \leq \frac{1}{c_m}$. [40].

Property 3: $|G(q)| \leq c_g$, where $c_g \in \mathbb{R}_{>0}$ is a known constant [40].

Property 4: $|P(q, \dot{q})| \leq c_{p1} + c_{p2}|\dot{q}|$, where $c_{p1}, c_{p2} \in \mathbb{R}_{>0}$ are known constants [41], [42], [43], [44].

Property 5: The control effectiveness of the motors are bounded as $\underline{B} \leq B_n \leq \overline{B}$, $\forall n$, where $\underline{B}, \overline{B} \in \mathbb{R}_{>0}$ are known constants [44].

Property 6: $c_j \leq J_n \leq c_J, \forall n$, where $c_j, c_J \in \mathbb{R}_{>0}$ are known constants. [40]

Property 7: $|D_n| \leq c_D, \forall n$, where $c_D \in \mathbb{R}_{>0}$ is a known constant. [40]

Assumption 1: $c_{\dot{m}} \leq \dot{M}(q) \leq c_{\dot{M}}$, where $c_{\dot{m}}, c_{\dot{M}} \in \mathbb{R}_{>0}$ are known constants [45], [46].

Assumption 2: $|d_n(t)| \leq c_d, \forall n$, where $c_d \in \mathbb{R}_{>0}$ is a known constant.

III. HIGH-LEVEL JOINT CONTROL DEVELOPMENT

The objective of the high-level control design is to track desired, periodic knee kinematic trajectories to move the shank in the extension and flexion directions. Thus, a repetitive learning controller inspired by [27] is developed for the high-level knee joint control objective.

To quantify the joint tracking objective, the position tracking and filtered tracking errors denoted by $\xi, \eta : \mathbb{R}_{\geq t_0} \to \mathbb{R}$ are defined as

$$\xi(t) \triangleq q_d(t) - q(t), \tag{5}$$

$$\eta(t) \triangleq \dot{\xi}(t) + \gamma\xi(t), \tag{6}$$

where $q_d, \dot{q}_d, \ddot{q}_d : \mathbb{R}_{\geq t_0} \to \mathbb{R}$ are bounded desired joint trajectories such that $|q_d| \leq \overline{q_d}$, $|\dot{q}_d| \leq \overline{\dot{q}_d}$, $|\ddot{q}_d| \leq \overline{\ddot{q}_d}$, where $\overline{q_d}, \overline{\dot{q}_d}, \overline{\ddot{q}_d} \in \mathbb{R}$ are known constants, and $\gamma \in \mathbb{R}_{>0}$ is a selectable control gain. The desired knee-joint trajectories are periodic in the sense that $q_d(t) = q_d(t - T)$, $\dot{q}_d(t) = \dot{q}_d(t - T)$, $\ddot{q}(t) = \ddot{q}_d(t - T)$ with a known period $T \in \mathbb{R}_{>0}$. The open-loop error system can be obtained by taking the time derivative of (6), pre-multiplying by M, substituting for (1), (2) and (5), and performing some algebraic manipulation to yield[1]

$$M\dot{\eta} = \chi - B_e u + W_d + N_d, \tag{7}$$

where the auxiliary signals $\chi, W_d, N_d \in \mathbb{R}$ are defined as

$$\chi \triangleq M(q)\left(\ddot{q}_d + \gamma\dot{\xi}\right) + G(q) + P(q, \dot{q}) - W_d - N_d, \tag{8}$$

$$W_d \triangleq M(q_d)\ddot{q}_d + G(q_d), \tag{9}$$

$$N_d \triangleq c_{p1} + c_{p2}\dot{q}_d. \tag{10}$$

By using Properties 1, 3 and 4, the mean value theorem and the explicit boundedness of the periodic desired trajectories, the auxiliary signals χ, W_d, N_d can be upper bounded as

$$|\chi| \leq \rho\|z\|, \tag{11}$$

$$|W_d| \leq \beta_\eta, \tag{12}$$

$$|N_d| \leq \Theta, \tag{13}$$

where $\rho, \beta_\eta, \Theta \in \mathbb{R}_{>0}$ are known positive constants, and the composite error vector $z : \mathbb{R}_{\geq t_0} \to \mathbb{R}^2$ is defined as

$$z \triangleq \begin{bmatrix} \xi & \eta \end{bmatrix}^T. \tag{14}$$

Given the open-loop error system in (7), the high-level control input $u : \mathbb{R}_{\geq t_0} \to \mathbb{R}$ can be designed as

$$u = \hat{W}_d + \psi_1\eta + \left(\psi_2 + \psi_3\|z\| + \psi_4|\hat{W}_d|\right)\text{sgn}(\eta), \tag{15}$$

where $\psi_1, \psi_2, \psi_3, \psi_4 \in \mathbb{R}_{>0}$ are selectable positive control gains. The designed control input u in (15) is composed of the repetitive learning term $\hat{W}_d$ that acts as a feedforward term exploiting the periodic nature of the desired knee trajectory, the feedback term $\psi_1\eta$ that exploits the instantaneous joint kinematic tracking error, and the sliding mode terms that compensate for the disturbances, the uncertain terms upper bounded by a constant in (13), the state-dependent uncertainty in (11), and the learning cross term that influence the high-level closed-loop error system. The repetitive learning control law $\hat{W}_d : \mathbb{R}_{\geq 0} \to \mathbb{R}$ is designed as [37]

$$\hat{W}_d(t) = \text{sat}_{w_1,w_2}\left(\hat{W}_d(t - T)\right) + \mu\eta(t), \tag{16}$$

where $\mu \in \mathbb{R}_{>0}$ is a control gain and T is the known time period of the desired leg trajectories. The saturation function $\text{sat}_{w_1,w_2}(\cdot)$ is defined as

$$\text{sat}_{w_1,w_2}(\cdot) \triangleq \begin{cases} w_1 & \text{for } (\cdot) \geq w_1 \\ (\cdot) & \text{for } w_1 > (\cdot) > w_2, \\ w_2 & \text{for } (\cdot) \leq w_2 \end{cases} \tag{17}$$

where $w_1 > w_2 \in \mathbb{R}$ are upper and lower bounds.

The closed-loop error system can be expressed by substituting (15) into (7) and performing some algebraic

[1] Functional dependencies are omitted henceforth, unless required for clarification.

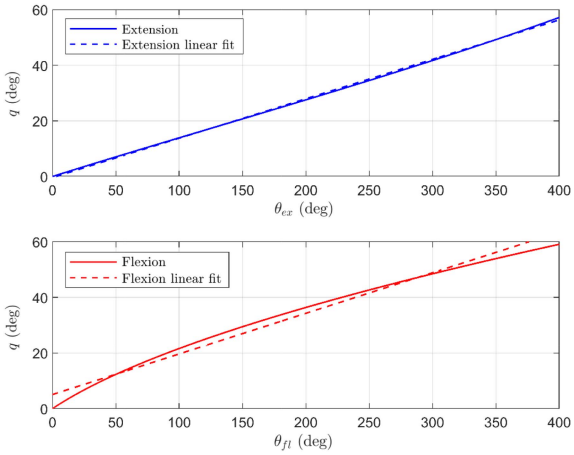

FIGURE 2. Experimental data depicting the knee joint angle q as a function of the leader motor angles $\theta_{\bar{n}}$, for $\bar{n} \in \{ex, fl\}$ of the extension motor (solid blue line) and flexion motor (solid red line). The dashed lines are the linear fit for the extension (blue) and flexion (red) motors with goodness of fit $R^2 = 0.9969$ and $R^2 = 0.9809$, respectively.

manipulation as

$$M\dot{\eta} = \chi + \tilde{W}_d + \hat{W}_d + N_d - B_e\left(\hat{W}_d + \psi_1\eta + \left(\psi_2 + \psi_3\|z\| + \psi_4|\hat{W}_d|\right)\operatorname{sgn}(\eta)\right), \tag{18}$$

where the unknown learning estimation error $\tilde{W}_d \in \mathbb{R}$ is defined as $\tilde{W}_d \triangleq W_d - \hat{W}_d$. Due to the periodicity and boundedness of $W_d(t)$, the following relationship is derived

$$W_d(t) = \text{sat}_{w_1,w_2}(W_d(t)) = \text{sat}_{w_1,w_2}(W_d(t-T)), \tag{19}$$

and the learning estimation error $\tilde{W}_d$ can be expressed as

$$\tilde{W}_d(t) = \text{sat}_{w_1,w_2}(W_d(t-T)) - \text{sat}_{w_1,w_2}\left(\hat{W}_d(t-T)\right) - \mu\eta, \tag{20}$$

using the repetitive learning update law in (16).

IV. LOW-LEVEL FOLLOWER MOTOR CONTROL DEVELOPMENT

The objective of the low-level follower motor control design is to mitigate cable slackness and prevent counteracting forces with the leader motor. To quantify the performance of the follower motor, the measurable error for each motor $e_n : \mathbb{R}_{\geq t_0} \to \mathbb{R}, \forall n$, can be defined as

$$e_n(t) = \theta_{\bar{n}}(t) - \theta_n(t) + \alpha\delta_n(t), \forall n, \tag{21}$$

where $\alpha \in \mathbb{R}_{>0}$ is a selectable constant control gain, and the subscript $\bar{n}$ denotes the complementary motor for motor n (e.g., if $n = ex$, then $\bar{n} = fl$, and vice versa).

Remark 1: As depicted in Fig. 2 , when a motor is serving as a leader motor, the state-dependent and time-invariant mapping between the knee joint angle q and the corresponding motor's angular position $\theta_{\bar{n}}$ denoted by $\phi_{\bar{n}} : \mathbb{R}_{\geq t_0} \to \mathbb{R}$ exists, and can be defined as

$$\phi_{\bar{n}}(\theta_{\bar{n}}) = v_{\bar{n}}\theta_{\bar{n}} + w_{\bar{n}} = q, \forall \bar{n}, \tag{22}$$

where $v_{\bar{n}}, w_{\bar{n}} \in \mathbb{R}$ are known constants based on the geometry of the exoskeleton design.

The target offset angles, velocities, and accelerations for both motors can be expressed as $\delta_n, \dot{\delta}_n, \ddot{\delta}_n : \mathbb{R}_{\geq t_0} \to \mathbb{R}, \forall n$, which are generated from the following admittance models:

$$M_a\ddot{\delta}_{ex} + D_a\dot{\delta}_{ex} + K_a\delta_{ex} = \text{sat}_{a_1,a_2}\left(k_T(T_{ex} - T_d)^3\right), \tag{23}$$

$$M_a\ddot{\delta}_{fl} + D_a\dot{\delta}_{fl} + K_a\delta_{fl} = \text{sat}_{a_3,a_4}\left(k_T(T_d - T_{fl})^3\right). \tag{24}$$

The desired virtual mass, damper, and stiffness parameters are denoted as $M_a, D_a, K_a \in \mathbb{R}_{>0}$. The parameters in (23) and (24) are selected such that the transfer functions are passive[47, Lemma 6.4]. The measurable cable tension signals corresponding to the cables connected to the extension and flexion motors are denoted as $T_{ex}, T_{fl} : \mathbb{R}_{\geq t_0} \to \mathbb{R}$, which are bounded with bounded u and $u_n, \forall n$. The desired cable tension is denoted as $T_d \in \mathbb{R}_{>0}$, and the selectable parameters in the admittance model are denoted as $a_1, a_2, a_3, a_4, k_T \in \mathbb{R}$. The saturation functions $\text{sat}_{a_1,a_2}(\cdot)$ and $\text{sat}_{a_3,a_4}(\cdot)$ are defined similarly to (17) using their corresponding upper and lower bounds.

The filtered tracking error for each motor $r_n : \mathbb{R}_{\geq t_0} \to \mathbb{R}, \forall n$, can be defined as

$$r_n(t) = \dot{e}_n(t) + \beta e_n(t), \forall n, \tag{25}$$

where $\beta \in \mathbb{R}_{>0}$ is a selectable constant control gain. Taking the time derivative of (25), pre-multiplying by J_n, substituting for (4) and (21), and performing some algebraic manipulation yields

$$J_n\dot{r}_n = J_n\ddot{\theta}_{\bar{n}} + D_n\dot{\theta}_n + d_n - B_nu_n - e_n + J_n\alpha\ddot{\delta}_n + J_n\beta\dot{e}_n + e_n. \tag{26}$$

Taking the time derivative of (22) twice and substituting into (1), and then substituting it into the previous equation yields

$$J_n\dot{r}_n = \chi_n - B_nu_n + J_n\left(\frac{B_e}{v_{\bar{n}}}M^{-1}u + \alpha\ddot{\delta}_n\right) - e_n, \tag{27}$$

where the auxiliary signal $\chi_n : \mathbb{R}_{\geq t_0} \to \mathbb{R}, \forall n$, is defined as

$$\chi_n = J_n\left[\frac{1}{v_{\bar{n}}}M^{-1}(-G - P) + \beta\dot{e}_n\right] + D_n\dot{\theta}_n + d_n + e_n. \tag{28}$$

Using Properties 1–4, Properties 6–7, and Assumption 2, the auxiliary signal can be bounded as

$$|\chi_n| \leq c_{n,1} + c_{n,2}\|l_n\|, \forall n, \tag{29}$$

where $c_{n,1}, c_{n,2} \in \mathbb{R}_{\geq 0}, \forall n$, are known constants, and $l_n : \mathbb{R}_{\geq t_0} \to \mathbb{R}, \forall n$, is defined as

$$l_n \triangleq \begin{bmatrix}\xi & \eta & e_n & r_n\end{bmatrix}^T. \tag{30}$$

The low-level follower motor control input can be designed as

$$u_n = k_{n,1} r_n + \left(k_{n,2} + k_{n,3}\|l_n\| + k_{n,4}|u| + k_{n,5}|\ddot{\delta}_n|\right) \operatorname{sgn}(r_n), \tag{31}$$

where $k_{n,1}, k_{n,2}, k_{n,3}, k_{n,4}, k_{n,5} \in \mathbb{R}_{>0}, \forall n$, are positive selectable control gains. The designed control input u_n in (31) is composed of a feedback term $k_{n,1} r_n$ leveraging the instantaneous tracking error and the high-frequency control terms that are multiplied by the signum function to compensate for disturbances and the cross-terms due to the composite error l_n, the high-level control input u and the indirect force term $\ddot{\delta}_n$ that influence the low-level closed-loop error system.

Remark 2: Since the high-level knee joint control input u can be implemented separately in the high-level control loop using the knee joint kinematics, then the low-level control input u_n is implementable.

The closed-loop error system can be obtained by substituting (31) into (27) as

$$J_n \dot{r}_n = \chi_n - e_n - B_n\big[k_{n,1} r_n + \left(k_{n,2} + k_{n,3}\|l_n\| + k_{n,4}|u| + k_{n,5}|\ddot{\delta}_n|\right) \operatorname{sgn}(r_n)\big] + J_n\left(\frac{B_e}{v_{\bar{n}}} M^{-1} u + \alpha \ddot{\delta}_n\right). \tag{32}$$

V. STABILITY ANALYSIS

The stability of the high-level knee joint kinematic controller and low-level follower motor controller can be examined independently through the following two theorems. Theorem 1 shows that the closed-loop knee kinematic controller with repetitive learning achieves asymptotic tracking. Theorem 2 shows that the low-level robust follower motor controllers achieve exponential tracking. Lemma 1 is used to prove that the inactive low-level following motor controller is uniformly bounded.

Theorem 1: Given the closed-loop error system in (18), the high-level controller in (15) and repetitive learning control law in (16) ensures global asymptotic tracking in the sense that

$$\lim_{t \to \infty} \xi(t) = 0, \tag{33}$$

provided the following sufficient gain conditions are satisfied

$$\psi_1 > \frac{c_{\dot{M}} - \mu}{2\underline{B}}, \psi_2 \geq \frac{\Theta}{\underline{B}}, \psi_3 \geq \frac{\rho + 1}{\underline{B}}, \psi_4 \geq \frac{1 + \overline{B}}{\underline{B}}. \tag{34}$$

Proof: Let $V_h : \mathbb{R}^3 \times \mathbb{R}_{\geq t_0} \to \mathbb{R}$ be a positive-definite, continuously differentiable Lyapunov function candidate defined as

$$V_h = \frac{1}{2}\xi^2 + \frac{1}{2} M \eta^2 + \frac{1}{2\mu} \int_{t-T}^{t} \left(\operatorname{sat}_{w_1,w_2}\left(W_d(\varphi)\right) - \operatorname{sat}_{w_1,w_2}\left(\hat{W}_d(\varphi)\right)\right)^2 d\varphi, \tag{35}$$

which satisfies the following inequalities

$$\gamma_1 \|z_h\|^2 \leq V_h \leq \gamma_2 \|z_h\|^2, \tag{36}$$

where $\gamma_1 \triangleq \min\left(\frac{1}{2}, \frac{1}{2}c_m, \frac{1}{2\mu}\right)$, $\gamma_2 \triangleq \max\left(\frac{1}{2}, \frac{1}{2}c_M, \frac{1}{2\mu}\right)$, and $z_h \triangleq \begin{bmatrix} z^T & \mathcal{Z} \end{bmatrix}^T$, where

$$\mathcal{Z} \triangleq \sqrt{\int_{t-T}^{t} \left(\operatorname{sat}_{w_1,w_2}\left(W_d(\varphi)\right) - \operatorname{sat}_{w_1,w_2}\left(\hat{W}_d(\varphi)\right)\right)^2 d\varphi}. \tag{37}$$

Let $z_h(t)$ be a Filippov solution to the differential inclusion $\dot{z}_h \in K[h_1](z_h)$, where $K[\cdot]$ is an upper semi-continuous, nonempty, compact and convex valued map on $\mathcal{Q} \subset \mathbb{R}$, where $\mathcal{Q}$ is an open and connected set, as defined in [48], [49]. The vector h_1 is defined by using (5) and (6) as $h_1 \triangleq \begin{bmatrix} \dot{\xi} & M\dot{\eta} & \mathcal{H} \end{bmatrix}$, where

$$\mathcal{H} \triangleq \frac{1}{2\mathcal{Z}}\Big[\left(sat_{w_1,w_2}\left(W_d(t)\right) - sat_{w_1,w_2}\left(\hat{W}_d(t)\right)\right)^2 - \left(sat_{w_1,w_2}\left(W_d(t-T)\right) - sat_{w_1,w_2}\left(\hat{W}_d(t-T)\right)\right)^2\Big]. \tag{38}$$

Due to the sliding mode terms in (15), which induce a discontinuity at any point in $\mathcal{Q}$, then a generalized solution using Filippov solutions [48] at a certain point can be found by examining the behavior of its derivative at nearby points utilizing differential inclusions (i.e., since a solution to the system may not exist in the classical sense [49]). Hence, since the control input in (15) has the discontinuous signum function, the time derivative of (35) exists almost everywhere (a.e.), i.e., for almost all t. Based on [49, Lemma 1], the time derivative of (35), $\dot{V}_h(z_h(t), t) \overset{a.e.}{\in} \dot{\tilde{V}}_h(z_h(t), t)$, where $\dot{\tilde{V}}_h$ is the generalized time derivative of (35) along the Filippov trajectories of $\dot{z}_h = h_1(z_h)$ and is defined as in [49] as $\dot{\tilde{V}}_h \triangleq \bigcap_{\varsigma \in \partial V_h} \varsigma^T K[\begin{matrix} \dot{\xi} & \dot{\eta} & \mathcal{H} & 1 \end{matrix}]^T(\xi, \eta, \mathcal{Z}, t)$. Since $V_h(z_h, t)$ is continuously differentiable in z_h, $\partial V_h = \{\nabla V_h\}$, thus $\dot{\tilde{V}}_h \overset{a.e.}{\subset} [\begin{matrix} \xi & M\eta & (\frac{1}{2\mu})2\mathcal{Z} & \frac{1}{2}\dot{M}\eta^2 \end{matrix}] K [\begin{matrix} \dot{\xi} & \dot{\eta} & \mathcal{H} & 1 \end{matrix}]^T$. After substituting for (5), (6), and (18), the generalized time derivative of (35) can be expressed as

$$\dot{\tilde{V}}_h \overset{a.e.}{\subset} -\gamma\xi^2 + \eta\xi + \frac{1}{2}\dot{M}\eta^2 + \eta\Big[\chi + \tilde{W}_d + \hat{W}_d + N_d - K[B_e]\Big(\hat{W}_d + \psi_1\eta + \left(\psi_2 + \psi_3\|z\| + \psi_4|\hat{W}_d|\right) K[\operatorname{sgn}(\eta)]\Big)\Big] + \frac{1}{2\mu}\left(sat_{w_1,w_2}\left(W_d(t)\right) - sat_{w_1,w_2}\left(\hat{W}_d(t)\right)\right)^2 - \frac{1}{2\mu}\left(sat_{w_1,w_2}\left(W_d(t-T)\right) - sat_{w_1,w_2}\left(\hat{W}_d(t-T)\right)\right)^2, \tag{39}$$

where $K[\operatorname{sgn}(\cdot)] = SGN(\cdot)$ such that $SGN(\cdot) = 1$ if $(\cdot) > 0$; $[-1, 1]$ if $(\cdot) = 0$; -1 if $(\cdot) < 0$. Substituting for (11), (12), (13), (20), exploiting Property 5, using Assumption 1 and performing some algebraic manipulation, the expression in

(39) can be upper bounded as

$$\dot{\tilde{V}}_h \overset{a.e.}{\leq} -\gamma\xi^2 + \left(\frac{1}{2}c_{\dot{M}} - \underline{B}\psi_1\right)\eta^2 + \eta\tilde{W}_d + |\eta|\left|\hat{W}_d\right|\left(1 + \bar{B} - \underline{B}\psi_4\right) + |\eta|\left(-\underline{B}\psi_2 + \Theta\right) + |\eta|\,\|z\|\left(-\underline{B}\psi_3 + \rho + 1\right) - \frac{1}{2\mu}\left(\tilde{W}_d + \mu\eta\right)^2 + \frac{1}{2\mu}\left(sat_{w_1,w_2}\left(W_d(t)\right) - sat_{w_1,w_2}\left(\hat{W}_d(t)\right)\right)^2. \tag{40}$$

The inequality in (40) can be further upper bounded by employing the property in [37, Appendix I], to yield

$$\dot{\tilde{V}}_h \overset{a.e.}{\leq} -\gamma\xi^2 + \left(\frac{1}{2}c_{\dot{M}} - \underline{B}\psi_1 - \frac{1}{2}\mu\right)\eta^2 + |\eta|\left(-\underline{B}\psi_2 + \Theta\right) + |\eta|\,\|z\|\left(-\underline{B}\psi_3 + \rho + 1\right) + |\eta|\left|\hat{W}_d\right|\left(1 + \bar{B} - \underline{B}\psi_4\right). \tag{41}$$

Provided the sufficient gain conditions in (34), the previous inequality can be further upper bounded as

$$\dot{\tilde{V}}_h \overset{a.e.}{\leq} -\gamma\xi^2 + \left(\frac{1}{2}c_{\dot{M}} - \underline{B}\psi_1 - \frac{1}{2}\mu\right)\eta^2 \overset{a.e.}{\leq} -\lambda_h\|z\|^2, \tag{42}$$

where $\lambda_h \triangleq \min\{\gamma, (\frac{1}{2}c_{\dot{M}} - \underline{B}\psi_1 - \frac{1}{2}\mu)\}$. Using [49, Corollary 2], $|\xi|, |\eta| \to 0$ as $t \to \infty$. Since $V_h \geq 0$ and $\dot{V}_h \leq 0$, $V_h \in \mathcal{L}_\infty$, thus, $\xi, \eta, \mathcal{Z} \in \mathcal{L}_\infty$. From (16), $\hat{W}_d \in \mathcal{L}_\infty$, and along with the fact that $W_d \in \mathcal{L}_\infty$ due to the periodicity and boundedness as shown in (12), $\tilde{W}_d \in \mathcal{L}_\infty$. Since $\xi, \dot{\xi}, \eta \in \mathcal{L}_\infty$, then $q, \dot{q} \in \mathcal{L}_\infty$ since $q_d, \dot{q}_d \in \mathcal{L}_\infty$, and thus, $u \in \mathcal{L}_\infty$. Then, $\ddot{q} \in \mathcal{L}_\infty$ in (1). ■

Theorem 2: Given the closed-loop error system in (32), the low-level motor follower controller in (31) ensures global exponential tracking in the sense that

$$\|z_n(t)\| \leq \sqrt{\frac{\gamma_4}{\gamma_3}}\|z_n(t_0)\|\exp\left(-\frac{\lambda_n}{2\gamma_4}(t - t_0)\right), \tag{43}$$

$\forall t \in (t_0, \infty)$, where $\lambda_n \triangleq \min\{\beta, \underline{B}k_{n,1}\}$, provided the following sufficient gain conditions are satisfied

$$k_{n,2} \geq \frac{c_{n,1}}{\underline{B}}, k_{n,3} \geq \frac{c_{n,2}}{\underline{B}}, k_{n,4} \geq \frac{c_J\bar{B}}{\underline{B}\upsilon_{\bar{n}}c_m}, k_{n,5} \geq \frac{c_J\alpha}{\underline{B}}. \tag{44}$$

Proof: Let $V_n : \mathbb{R}^2 \times \mathbb{R}_{\geq t_0} \to \mathbb{R}$ be a positive-definite, continuously differentiable Lyapunov function candidate defined as

$$V_n = \frac{1}{2}e_n^2 + \frac{1}{2}J_n r_n^2, \tag{45}$$

which satisfies the following inequalities

$$\gamma_3\|z_n\|^2 \leq V_n \leq \gamma_4\|z_n\|^2, \tag{46}$$

where $\gamma_3 \triangleq \min(\frac{1}{2}, \frac{1}{2}c_j)$, $\gamma_4 \triangleq \max(\frac{1}{2}, \frac{1}{2}c_J)$, and $z_n \triangleq [\ e_n \quad r_n\ ]^T$, $\forall n$. Let $z_n(t)$ be a Filippov solution to the differential inclusion $\dot{z}_n \in K[h_2](z_n)$, where $K[\cdot]$ is defined as in [50] and h_2 is defined by using (25) and (31) as $h_2 \triangleq [\ \dot{e}_n \quad J_n\dot{r}_n\ ]$. The low-level follower control input in (31) has the signum function; hence, the time derivative of (45) exists almost everywhere (a.e.), i.e., for almost all t. Based on [49, Lemma 1], the time derivative of (45), $\dot{V}_n(z_n(t), t) \overset{a.e.}{\in} \dot{\tilde{V}}_n(z_n(t), t)$, where $\dot{\tilde{V}}_n$ is the generalized time derivative of (45) along the Filippov trajectories of $\dot{z}_n = h_2(z_n)$ and is defined as in [49] as $\dot{\tilde{V}}_n \triangleq \bigcap_{\varsigma\in\partial V_n}\varsigma^T K[\ \dot{e}_n \quad \dot{r}_n\ ]^T(e_n, r_n)$. Since $V_n(z_n, t)$ is continuously differentiable in z_n, $\partial V_n = \{\nabla V_n\}$, thus $\dot{\tilde{V}}_n \overset{a.e.}{\subset} [\ e_n \quad J_n r_n\ ]K\ [\ \dot{e}_n \quad \dot{r}_n\ ]^T$. After substituting for (25) and (32), and canceling common terms, the generalized time derivative of (45) can be expressed as

$$\dot{\tilde{V}}_n \overset{a.e.}{\subset} e_n(r_n - \beta e_n) + r_n[\chi_n - e_n - B_n\left(k_{n,1}r_n + \left(k_{n,2} + k_{n,3}\|l_n\| + k_{n,4}|u| + k_{n,5}|\ddot{\delta}_n|\right)K[\mathrm{sgn}(r_n)]\right) + J_n\left(\frac{B_e}{\upsilon_{\bar{n}}}M^{-1}u + \alpha\ddot{\delta}_n\right)]. \tag{47}$$

Substituting for (29), and exploiting Properties 5-6, the expression in (47) can be upper bounded as

$$\dot{\tilde{V}}_n \overset{a.e.}{\leq} -\beta e_n^2 - \underline{B}k_{n,1}r_n^2 + |r_n|\left(c_{n,1} - \underline{B}k_{n,2}\right) + |r_n|\|l_n\|\left(c_{n,2} - \underline{B}k_{n,3}\right) + |r_n||u|\left(\frac{c_J\bar{B}}{\upsilon_{\bar{n}}c_m} - \underline{B}k_{n,4}\right) + |r_n||\ddot{\delta}_n|\left(c_J\alpha - \underline{B}k_{n,5}\right). \tag{48}$$

Provided the sufficient gain conditions in (44), the previous inequality can be further upper bounded as

$$\dot{\tilde{V}}_n \overset{a.e.}{\leq} -\beta e_n^2 - \underline{B}k_{n,1}r_n^2 \overset{a.e.}{\leq} -\lambda_n\|z_n\|^2, \tag{49}$$

where $\lambda_n \triangleq \min\{\beta, \underline{B}k_{n,1}\}$. Leveraging (46) and (49), the exponential tracking result in (43) can be obtained. Since, $V_n \geq 0$ and $\dot{V}_n \leq 0$, $V_n \in \mathcal{L}_\infty$, thus, $e_n, r_n \in \mathcal{L}_\infty$. Based on Theorem 1, the high-level control input $u \in \mathcal{L}_\infty$, and the high-level error signals $\xi, \eta, q \in \mathcal{L}_\infty$. And along with the fact that (23) and (24) are passive, then, $l_n, u_n \in \mathcal{L}_\infty$. The leader motor's angle $\theta_{\bar{n}} \in \mathcal{L}_\infty$ from (22) and together with $\delta_n \in \mathcal{L}_\infty$ in (23) and (24), $\theta_n \in \mathcal{L}_\infty$. Finally, $\ddot{\theta}_n \in \mathcal{L}_\infty, \forall n$ in (4). ■

Lemma 1: The low-level motor follower controller in (31) is uniformly bounded when inactive since

$$V_{\bar{n}} \in \mathcal{L}_\infty, \forall\bar{n}. \tag{50}$$

Proof: When motor $\bar{n}$ is the leader motor, its low-level motor follower controller is inactive (meaning, motor $\bar{n}$ is using the high-level control input u) to achieve the joint tracking objective. According to Theorem 1, the high-level control input $u \in \mathcal{L}_\infty$, and thus the high-level error signals $\xi, \eta, q \in \mathcal{L}_\infty$. The motor n is the follower motor and ensures $\theta_{\bar{n}}, \theta_n, e_n, r_n \in \mathcal{L}_\infty$ by Theorem 2. Hence, the inactive low-level follower controller of motor $\bar{n}$ will remain bounded $\chi_{\bar{n}}, V_{\bar{n}} \in \mathcal{L}_\infty, \forall\bar{n}$.■

VI. EXPERIMENTS

A. EXPERIMENTAL SETUP AND PROTOCOL

Experiments in six able-bodied individuals (five males aged 22-30 years and one female aged 22 years) were conducted

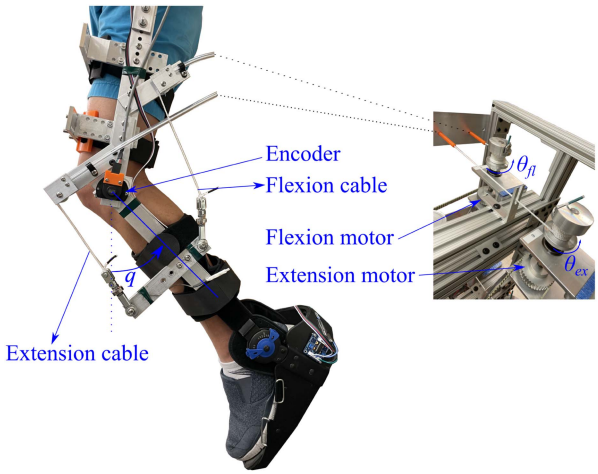

FIGURE 3. The cable-driven exoskeleton uses electric motors to actuate flexion and extension cables to apply torque at the knee joint. The motors are mounted on an external actuation unit to minimize the weight of the exoskeleton worn by participants.

to illustrate the performance of the developed controllers in (15) and (31), and repetitive learning control law in (16). Written informed consent was obtained prior to participation as approved by the Institutional Review Board at Syracuse University. Participants wore a cable-driven leg exoskeleton in a standing position, while the electric motors applied torque at the knee joint to achieve knee extension and flexion. Fig. 3 illustrates the exoskeleton testbed with 2 brushless 24 VDC electric motors (EC60 flat, Maxon) mounted on an external actuation unit used to actuate a cable-driven mechanism and apply torque about the knee joint. The angles of each motor $\theta_n, \forall n$, and knee joint q were measured using optical encoders (H1, US Digital). Load-cells (OMEGA) were installed in series with the cables to measure cable tension $T_n, \forall n$. The controllers were implemented on a desktop computer (Windows 10 OS) running a real-time target (QUARC 2.6, Quanser) via MATLAB/Simulink 2018a (MathWorks Inc) with a sample rate of 1 kHz. A Quanser QPIDe and a Q-8 DAQ boards were used to read the encoders and control the motor drivers (Maxon) operating in current-controlled mode.

Two trials were implemented for each individual with two different low-level controllers (Controller A and B) to compare the tracking performance with and without using the cable tension feedback to update the desired low-level motor follower trajectories, respectively. Controller A is the low-level controller designed in (31) with error signals e_n, r_n in (21) and (25), respectively, that leverage cable tension feedback through the use of the admittance models (23) and (24). Controller B is the low-level controller that does not use cable tension feedback developed in [38], in which the error signals are implemented as

$$e_n(t) = \theta_{\bar{n}}(t) - \theta_n(t), \tag{51}$$

$$r_n(t) = \dot{e}_n(t) + \beta e_n(t), \tag{52}$$

TABLE 1. Gains selection for high-level controller, low-level motor follower controller, and admittance models.

High-level Controller	γ	15	ψ_1	0.7
	μ	0.2	ψ_2	0.05
	w_1	2	ψ_3	7×10^{-4}
	w_2	-2	ψ_4	5×10^{-5}
Low-level Controller	α	4	β	30
	$k_{ex,1}$	6×10^{-3}	$k_{fl,1}$	8×10^{-3}
	$k_{ex,2}$	0.1	$k_{fl,2}$	0.1
	$k_{ex,3}$	5×10^{-5}	$k_{fl,3}$	5×10^{-5}
	$k_{ex,4}$	0.08	$k_{fl,4}$	0.1
	$k_{ex,5}$	5×10^{-4}	$k_{fl,5}$	2×10^{-4}
Admittance Model	a_1	2	M_a	0.5
	a_2	-22	D_a	6.5
	a_3	18	K_a	10
	a_4	-3	T_d	2

and thus, the low-level motor follower control inputs (Controller B) is designed as

$$u_n = k_{n,1} r_n + \left(k_{n,2} + k_{n,3}\|l_n\| + k_{n,4}|u|\right) \text{sgn}(r_n), \forall n, \tag{53}$$

respectively. It is noticeable that Controller B tracks the leader motor's kinematics and does not exploit cable tension feedback, i.e., δ_n is not used to compute e_n in (51), which is equivalent to setting $\alpha = 0$ in (21) and $k_{n,5} = 0$ in (31). Hence, the admittance models in (23) and (24) are not leveraged in the implementation of Controller B.

Leveraging the knee-joint range of motion obtained in previous work for treadmill walking [51], the range of the desired knee angle trajectory was defined between 10 to 50 degrees with a period of $T = 3$ seconds as depicted in Fig. 4 (top row plots). The sinusoid desired trajectory was implemented to test the repeatability of the developed control methods in multiple participants, prior to the implementation of the controllers in complex gait experiments. This trajectory also facilitates a standardized and consistent protocol to draw comparisons between the Controller A and Controller B across participants. The experiments are implemented with a duration of 60 seconds (20 leg swings in total).

B. CONTROL GAINS SELECTION

Table 1 includes the selection of the control gains for the high-level knee joint kinematic controller in (6), (15) and (16), the gains for the low-level follower control inputs (for both Controller A and Controller B) in (21), (25), (31), (52), and (53), and the parameters of the admittance models in (23) and (24).

C. TRACKING RESULTS

Table 2 summarizes the knee joint tracking error, follower motors tracking errors, and the cable tension performance for each participant with Controller A and B. The knee joint tracking performance and the high-level control input u for Subject 1 are presented in Fig. 4, where the desired knee joint trajectory q_d is depicted in blue, the actual knee joint angle q is depicted in red, and the knee joint tracking error ξ is depicted

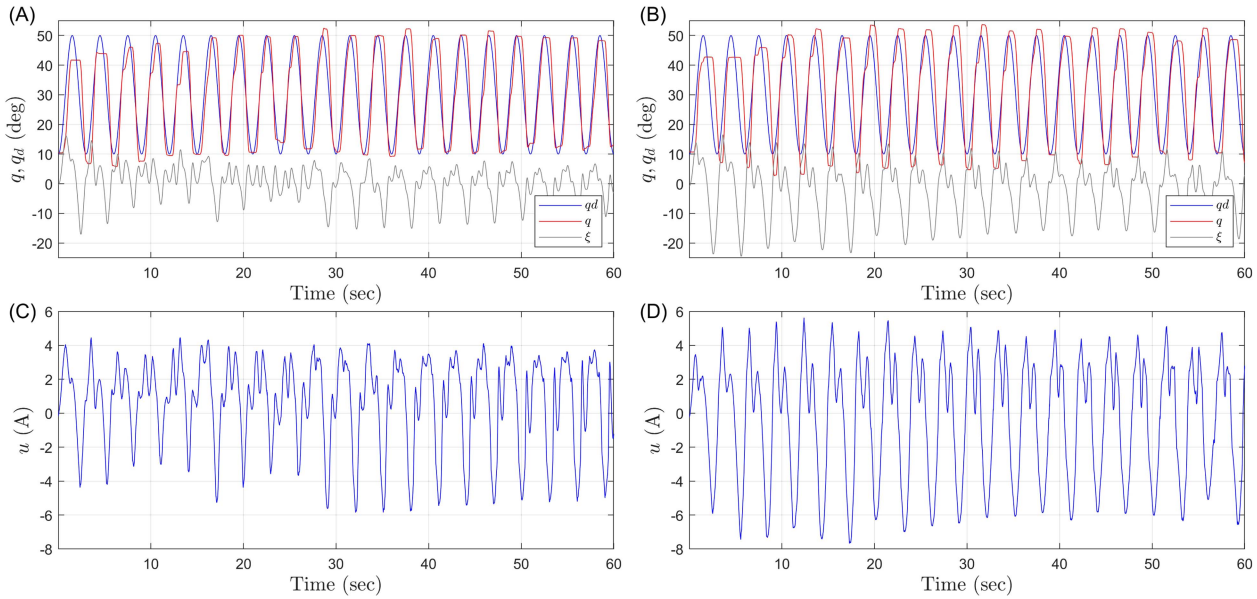

FIGURE 4. High-level knee joint tracking performance and high-level control input u for Subject 1 (S1). The left (a), (c) and right (b), (d) columns correspond to the performance of Controller A and Controller B, respectively. The top figures (A,B) depict joint angle performance comparing the desired trajectory q_d (blue) and the actual knee joint position q (red), and the knee joint tracking error ξ (gray). Bottom figures (c), (d) depict the high-level control input u for the two trials.

TABLE 2. Tracking results for each participant: high-level knee joint tracking error, low-level motor tracking error, and cable tension slackness with low-level controller A and B.

Tracking Error	Knee joint ξ (deg)[1]		Extension motor as follower motor e_{ex} (rad)[2]		Flexion motor as follower motor e_{fl} (rad)[2]		Extension cable slackness (%)[3]		Flexion cable slackness (%)[3]	
Controller	A	B	A	B	A	B	A	B	A	B
Subject										
S1	-0.15±5.47	-2.11±8.3	0.04±2.08	2.08±2.26	-3.33±2.58	-3.09±2.91	20.74	12.56	1.31	0.23
S2	2.00±4.95	-1.27±7.22	-0.02±2.17	2.49±1.59	-3.90±1.71	-3.12±2.64	27.23	29.87	0.70	0.00
S3	0.51±5.66	-0.66±6.58	0.38±1.94	1.27±1.51	-3.29±2.51	-3.06±3.1	24.88	46.90	5.64	0.00
S4	3.95±5.05	4.47±9.48	-0.54±2.15	0.95±1.37	-3.61±2.05	-1.21±1.97	42.56	51.76	0.48	0.00
S5	0.75±4.91	1.72±7.14	0.12±1.61	1.08±1.58	-3.28±2.09	-1.81±2.61	26.12	50.79	1.92	0.03
S6	1.55±3.67	0.36±4.99	-0.18±2.02	0.92±1.49	-2.60±1.67	-1.74±2.24	22.20	48.00	1.09	0.97
Mean	1.44	0.42	-0.03	1.47	-3.34	-2.34	27.29	39.98	1.86	0.21
STD	4.95	7.29	2.00	1.63	2.10	2.58	NA	NA	NA	NA

[1] The joint tracking error (mean± STD) is computed starting from the 4^{th} cycle at which the system reached steady-state performance.
[2] The motor position tracking error (mean± STD) was evaluated when the low-level follower controllers are active for the extension (ex) and flexion (fl) motors.
[3] Indicates the percentage of total time the cable experiences slackness, i.e., $\frac{\sum t \in (T_n < T_d)}{\sum t}$. A low percentage indicates the cable is experiencing slackness for low periods of time.

in gray. Fig. 5 shows the high-level control input u computed by Controllers A and B, where the red curves indicate the mean input u across the six participants and the shaded areas depict the standard deviation. The repetitive learning control law $\hat{W}_d$ defined in (16) is presented in Fig. 6 for Subject 1. The low-level follower motor tracking performance for Subject 1 is illustrated in Fig. 7, where the desired trajectory is depicted in red and the actual motor angle is depicted in blue. Fig. 8 illustrates the mean of the measured cable tension T_n, $\forall n$ across the six participants, and the shaded areas depict the standard deviation.

VII. DISCUSSION

The experimental results demonstrate the feasibility of the developed low-level follower controllers designed in (31) to mitigate cable slackness and counteracting forces while the high-level controller in (15) to achieve satisfactory knee joint tracking performance. In the previous theoretical work [38], the objective of the low-level follower controller is to activate the complementary motor to closely follow the kinematics of the leader motor. This controller ensures the motors are tracking close to each other; however, the lack of feedback of the actual cable tension limits the capacity to cope with

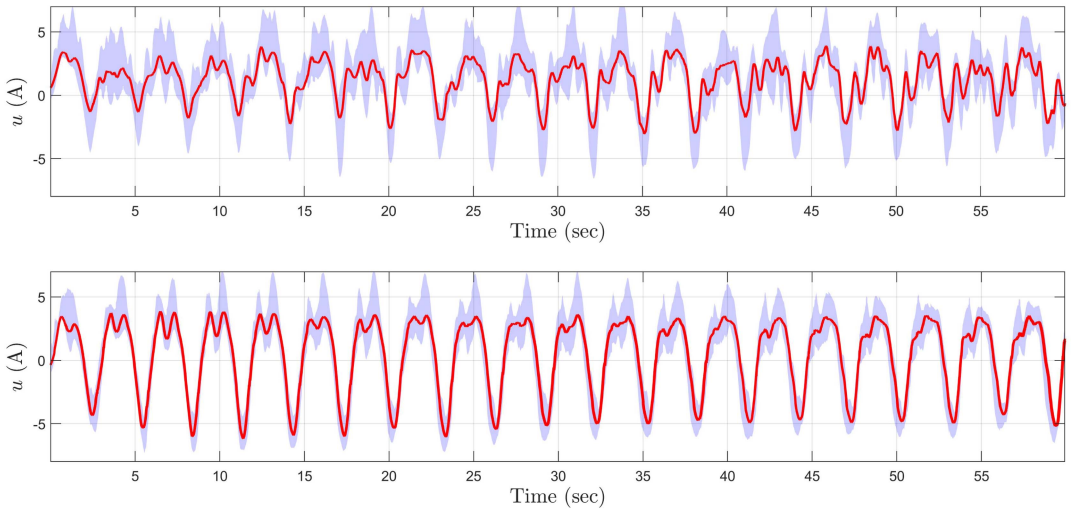

FIGURE 5. High-level control inputs u across all subjects for both trials (with low-level Controller A and Controller B). The top figure corresponds to the Controller A and the bottom figure corresponds to Controller B, respectively. The light blue area indicates the standard deviation of the mean control input and the red curve indicates the mean input for all subjects.

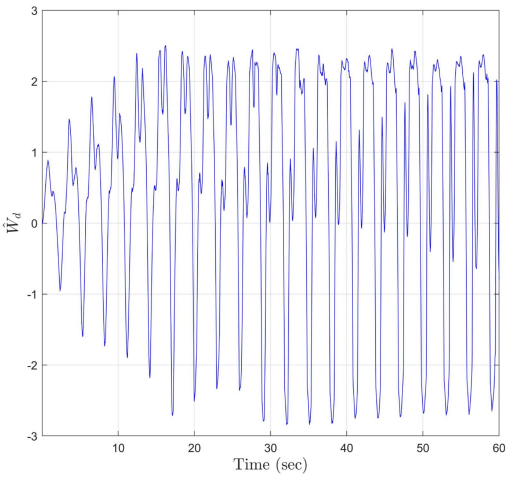

FIGURE 6. Repetitive learning control input $\hat{W}_d$ during the experiment of Subject 1 (S1) with Controller A. The update law is initialized to 0 and is computed using (16) to learn the periodic dynamics exploiting the fact that leg swings (knee flexion and extension) are periodic with period $T = 3$ seconds.

slackness and thus, adjust the cable tension correspondingly. The low-level follower controllers in this article directly exploit cable tension feedback to mitigate cable slackness and counteracting forces. The desired trajectory for the follower motor n includes not only the complementary motor $\bar{n}$ kinematics, but also the kinematic offset motor angle δ_n, which is generated from the admittance models in (23) and (24) that leverage the cable tension measurements to adjust the cable tension indirectly (i.e., through indirect force control). To demonstrate the improvement in tracking performance, low-level Controllers A and B were implemented in each participant with the same high-level controller u in (15).

A. HIGH-LEVEL KNEE JOINT TRACKING PERFORMANCE

The mean knee joint position error is 1.44 deg and 0.42 deg across participants for Controllers A and B, respectively. The average knee joint tracking error is not significantly different between the two controllers, but Controller A has less average standard deviation compared to Controller B. The knee joint tracking performance for Subject 1 is presented in Fig. 4 to compare the two controllers. The high-level joint controller in (15) smoothly brought the knee joint angle to track the desired steady-state within 4 cycles. The repetitive learning control input $\hat{W}_d$ shown in Fig. 6 illustrates the learning of the periodic dynamics during the leg swings. The repetitive learning control term adjusts the control input due to the periodicity of the leg motion and exploits the inputs recorded in the previous iteration.

With the same high-level controller u, the joint tracking error (difference between q_d and q) obtained with the low-level Controller B [Fig. 4(b)] is bigger and the joint angle has a larger variation than the joint performance obtained with the low-level Controller A [Fig. 4(a)], despite the fact that the mean tracking errors for both low-level controllers are similar. In Fig. 4, the high-level control input u has a larger magnitude range with low-level Controller B [Fig. 4(d)] than low-level Controller A [Fig. 4(c)] for Subject 1. To demonstrate this larger variability of u with the implementation of the low-level Controller B, Fig. 5 shows the average high-level control input u for all participants for both controllers. The experimental results indicate that the implementation of different low-level controllers plays a relevant role in the high-level knee joint tracking results.

B. LOW-LEVEL MOTOR FOLLOWING PERFORMANCE

Fig. 7 presents the low-level motor tracking performance, where the red curves indicate the desired trajectories, the blue

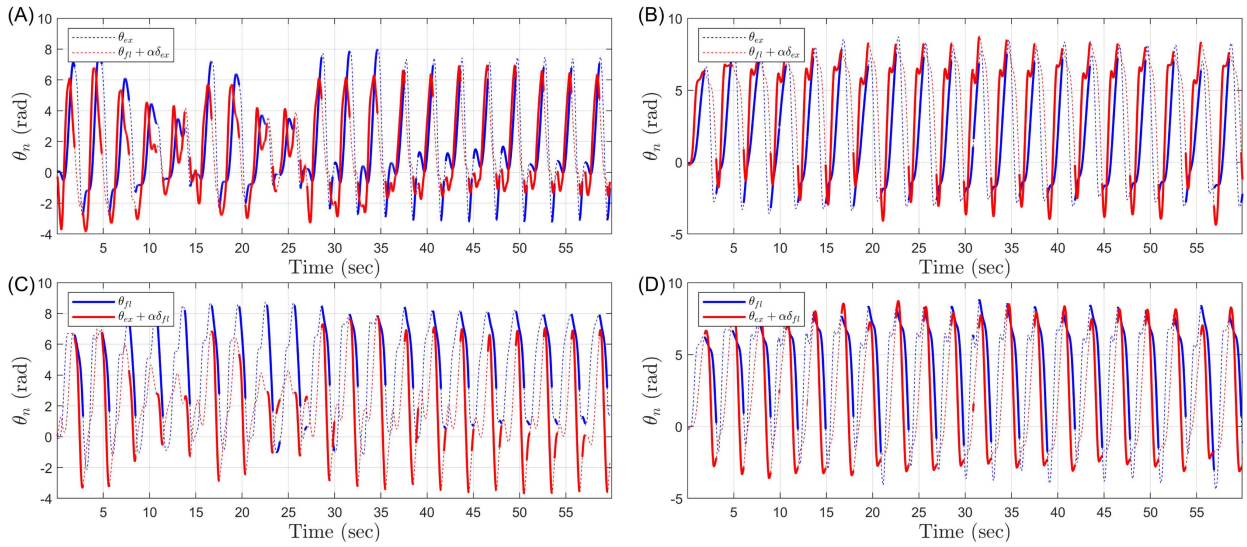

FIGURE 7. Low-level tracking performance of both extension (ex) and flexion (fl) motors for Subject 1 (S1). Figures of the performance of Controller A and Controller B are presented in left (a), (c) and right (b), (d) columns, respectively. Top (a), (b) and bottom (c), (d) figures depict the tracking performance of the extension and flexion motors, respectively. The desired trajectory is depicted in red, and the actual motor angle is depicted in blue for all plots. The dashed curves indicates when the low-level follower subsystem is inactive (thus, the high-level controller is commanded to such motor). At any given time, when the motor n is serving as a follower motor, the follower control for the complementary motor $\bar{n}$ is inactive (since motor $\bar{n}$ is receiving the control input u as the leader motor).

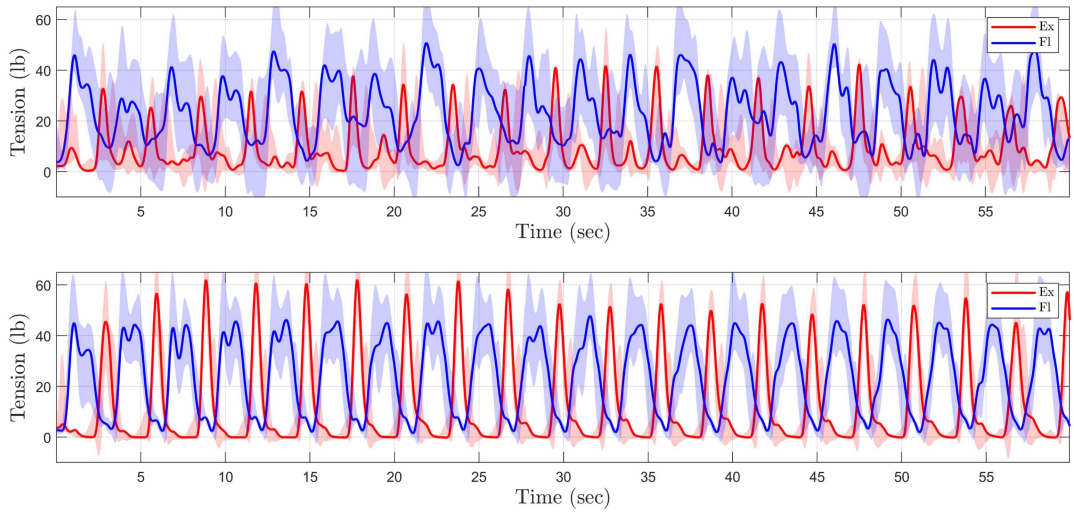

FIGURE 8. Cable tension measurements including all subjects. The tension measurements obtained in the experiment with Controller A and Controller B are presented in top and bottom figures, respectively. The average tension of the extension cable T_{ex} is depicted in blue, and the average tension of the flexion cable T_{fl} is depicted in red. The light area indicates the standard deviation of the cable tension including all subjects.

curves indicate the measured motor angles, and the dotted curves indicate when the low-level follower controller is inactive (e.g., such motor is the leader motor and receives u as its input). The average tracking errors for the Controller A corresponding to the extension and flexion motors are -0.03, -3.34 rad, respectively, while the average tracking errors for the Controller B are 1.47, -2.34 rad, respectively. Since the error signals e_n, r_n used in Controllers A and B are different (i.e., Controller A leverages (21) and (25), while Controller B uses (51) and (52)), it is not feasible to directly compare the low-level tracking performance between them since they fundamentally implement a different approach (e.g., kinematic plus indirect force control versus only kinematic control). Controller B is purely tracking the leader motor, while Controller A further includes the target offset angle δ_n computed from the admittance models. Overall, Controller A provides smaller control input magnitudes into the system and minimizes the standard deviation of the tracking performance compared to Controller B.

It is worth noting that the average tracking error is larger when the flexion motor is serving as a follower motor (i.e., when the knee is doing extension movement) for both

controllers. During experiments, the participants were standing upright and thus, the high-level controller lifted the shank to counteract the effects of gravity during the flexion movement. During the extension movement, the effect of gravity naturally aids the extension of the shank to reach the standing position, resulting typically in faster movements (compared to flexion motion). The high-level controller acts as a brake during knee extension, mitigating deviations from the desired trajectory due to gravity (and other disturbances). Consequently, the faster movement makes the flexion follower motor apply a larger input to follow the extension (leader) motor during knee extension. These observations are supported by the computed control inputs and tracking performance, where the average high-level control input u across all experiments are 2.54 A and -0.86 A in knee flexion and extension movement, respectively, and the larger tracking errors in Fig. 7(c) and (d).

C. CABLE TENSION AND SLACKNESS

Controllers A and B can also be examined based on the applied tension to achieve the tracking objective (e.g., in addition to the joint kinematic tracking performance). The measured cable tensions for both low-level controllers are illustrated in Fig. 8, where the percentage of the total time that each cable is experiencing slackness are 27.29(ex), 1.86(fl) and 39.98(ex), 0.21(fl) (%) for Controllers A and B, respectively. These percentages are computed as the summation of the time the cable is experiencing slackness ($T_n < T_d$) divided by the total time (see the percentages for all participants reported in Table 2). The target offset motor angle δ_n, $\forall n$, generated by the admittance model seeks to adjust the motor angle to maintain the cable tension close to the desired tension. The cable tensions are different between the two controllers in Fig. 8, where the average peak tension for the extension cable (red) is 42 lb for Controller A and 62 lb for Controller B. This additional cable tension demand computed by Controller B is partially due to cable slackness, which is happening in each swing period (when the cable tension reaches 0). When the cable slackness happens, the pulley system takes additional time to tension the cable while the controller increases the control input to minimize the error, and this results in higher pulling forces once the cable is finally tensioned (i.e., resulting in increased cable tension). As reported in Table 2, the difference between the mean extension cable slackness percentage of Controller A and Controller B is 12.69% (i.e., Controller A experiences slackness on average 12.69% less time than Controller B across all participants). For both controllers, the flexion cable experience slackness less than 2% of the total time (see the mean values across all participants in Table 2). Overall, Controller A successfully reduces the cable slackness and peak cable tension compared to Controller B. In addition, Controller A required less control effort than Controller B, which can aid mitigating unsafe actuator control forces applied to the lower-limb exoskeleton worn by participants.

D. SUMMARY

This article describes the design, analysis, implementation, and preliminary comparison of two low-level controllers for a cable-driven knee exoskeleton. The comparative analysis shows that Controller A exhibits several advantages over Controller B. First, Controller A demonstrates reduced variability in knee tracking error and requires less high-level control command, resulting in better tracking performance compared to Controller B. Second, Controller A shows a notable reduction in cable slackness compared to Controller B, and the peak cable tension is also lower than Controller B. Overall, the study demonstrates the benefits in performance of the new control design (Controller A) over the previously developed controller (Controller B) in [38]. Nevertheless, the selection of the control approach (e.g., a kinematic approach versus a kinematic plus an indirect force control approach) to be implemented for a given exoskeletal application is dependent on the availability of actuators, sensors, and computational resources to achieve a desired tracking objective. Ultimately, human perception of the control algorithm (e.g., tolerance of the applied forces by the device) is another important consideration for determining a suitable control approach using exoskeletons.

VIII. CONCLUSION

A two-layer control structure was developed for a lower-limb cable-driven exoskeleton to activate a pair of motors to achieve desired knee joint tracking. A repetitive learning controller was developed for the high-level controller to track periodic desired knee joint trajectories. The low-level controller was developed to mitigate the potential cable slackness and counteracting forces. The target trajectory for each motor is updated exploiting measurements of the cable tension in real-time. A Lyapunov-based stability analysis is developed to ensure global asymptotic tracking performance for the knee joint tracking objective. The low-level control subsystems achieve exponential tracking as demonstrated in the Lyapunov-based stability analysis, while a bounded and stable tracking performance is guaranteed under switching between both low-level control subsystems. The control algorithms are successfully implemented in real-time experiments in six able-bodied individuals comparing two different low-level controllers in separate trials (i.e., Controllers A and B). The experimental results illustrate the potential of the developed controllers to improve low-level and knee-joint tracking performance, while preventing potential cable slackness and reducing the peak cable tensions to achieve the tracking objectives. Future work includes leveraging the developed controllers for treadmill walking experiments by combining the hip and ankle joints together with the knee joint. In addition, a gait-phase detection algorithm is currently being developed to ensure smooth multi-joint coordination for walking. Future efforts also include developing an adaptive-based control extension to enhance the performance of the low-level

controllers during gait experiments. An adaptive admittance controller is also motivated for customizing the virtual mass, damper, and spring in the admittance model in real-time.

REFERENCES

[1] S. Kirshblum and V. W. Lin, *Spinal Cord Medicine*. Berlin, Germany: Springer Publishing Company, 2018.

[2] T. G. Hornby et al., "Clinical practice guideline to improve locomotor function following chronic stroke, incomplete spinal cord injury, and brain injury," *J. Neurologic Phys. Ther.*, vol. 44, no. 1, pp. 49–100, 2020.

[3] A. Rodríguez-Fernández, J. Lobo-Prat, and J. M. Font-Llagunes, "Systematic review on wearable lower-limb exoskeletons for gait training in neuromuscular impairments," *J. Neuroengineering Rehabil.*, vol. 18, no. 1, pp. 1–22, 2021.

[4] G. Lv, H. Zhu, and R. D. Gregg, "On the design and control of highly backdrivable lower-limb exoskeletons: A discussion of past and ongoing work," *IEEE Control Syst. Mag.*, vol. 38, no. 6, pp. 88–113, Dec. 2018.

[5] R. D. Reyes et al., "Effect of joint friction compensation on a "muscle-first" motor-assisted hybrid neuroprosthesis," *Front. Neurorobot.*, vol. 14, 2020, Art. no. 588950.

[6] S. R. Chang et al., "A muscle-driven approach to restore stepping with an exoskeleton for individuals with paraplegia," *J. Neuroengineering Rehabil.*, vol. 14, no. 1, pp. 1–12, 2017.

[7] K. A. Shorter, G. F. Kogler, E. Loth, W. K. Durfee, and E. T. Hsiao-Wecksler, "A portable powered ankle-foot orthosis for rehabilitation," *J. Rehabil. Res. Develop.*, vol. 48, no. 4, pp. 459–472, 2011.

[8] R. Chin et al., "A pneumatic power harvesting ankle-foot orthosis to prevent foot-drop," *J. Neuroengineering Rehabil.*, vol. 6, no. 1, pp. 1–11, 2009.

[9] M. B. Naf, K. Junius, M. Rossini, C. Rodriguez-Guerrero, B. Vanderborght, and D. Lefeber, "Misalignment compensation for full human-exoskeleton kinematic compatibility: State of the art and evaluation," *Appl. Mech. Rev.*, vol. 70, no. 5, pp. 1–19, 2018.

[10] X. Cui, W. Chen, X. Jin, and S. K. Agrawal, "Design of a 7-DOF cable-driven arm exoskeleton (CAREX-7) and a controller for dexterous motion training or assistance," *IEEE/ASME Trans. Mechatron.*, vol. 22, no. 1, pp. 161–172, Feb. 2017.

[11] G. M. Bryan, P. W. Franks, S. C. Klein, R. J. Peuchen, and S. H. Collins, "A hip–knee–ankle exoskeleton emulator for studying gait assistance," *Int. J. Robot. Res.*, vol. 40, no. 4/5, pp. 722–746, 2020.

[12] A. T. Asbeck, K. Schmidt, I. Galiana, D. Wagner, and C. J. Walsh, "Multi-joint soft exosuit for gait assistance," in *Proc. IEEE Int. Conf. Robot. Automat.*, 2015, pp. 6197–6204.

[13] T. Noda, T. Teramae, B. Ugurlu, and J. Morimoto, "Development of an upper limb exoskeleton powered via pneumatic electric hybrid actuators with bowden cable," in *Proc. IEEE/RSJ Int. Conf. Intell. Robots Syst.*, 2014, pp. 3573–3578.

[14] T. Lenzi, N. Vitiello, S. M. M. De Rossi, S. Roccella, F. Vecchi, and M. C. Carrozza, "NEUROExos: A variable impedance powered elbow exoskeleton," in *Proc. IEEE Int. Conf. Robot. Automat.*, 2011, pp. 1419–1426.

[15] R. Verhoeven, "Analysis of the workspace of tendon-based," Ph.D. dissertation, Duisburg Gerhard Mercator Univ., Duisburg, Germany, 2003.

[16] V. Potkonjak, B. Svetozarevic, K. Jovanovic, and O. Holland, "The puller-follower control of compliant and noncompliant antagonistic tendon drives in robotic systems," *Int. J. Adv. Robot. Syst.*, vol. 8, no. 5, pp. 143–155, 2011.

[17] Y. Yun, P. Agarwal, J. Fox, K. E. Madden, and A. D. Deshpande, "Accurate torque control of finger joints with UT hand exoskeleton through Bowden cable SEA," in *Proc. IEEE/RSJ Int. Conf. Intell. Robots Syst.*, 2016, pp. 390–397.

[18] F. Xiao, Y. Gao, Y. Wang, Y. Zhu, and J. Zhao, "Design and evaluation of a 7-DOF cable-driven upper limb exoskeleton," *J. Mech. Sci. Technol.*, vol. 32, no. 2, pp. 855–864, 2018.

[19] P. Agarwal and A. D. Deshpande, "Series elastic actuators for small-scale robotic applications," *J. Mechanisms Robot.*, vol. 9, no. 3, 2017, Art. no. 031016.

[20] Z. Li, B. Huang, Z. Ye, M. Deng, and C. Yang, "Physical human-robot interaction of a robotic exoskeleton by admittance control," *IEEE Trans. Ind. Electron.*, vol. 65, no. 12, pp. 9614–9624, Dec. 2018.

[21] Y. Guo, H. Wang, Y. Tian, and J. Xu, "Position/force evaluation-based assist-as-needed control strategy design for upper limb rehabilitation exoskeleton," *Neural Comput. Appl.*, vol. 34, no. 15, pp. 13075–13090, 2022.

[22] B. Brahmi, M. Saad, M. H. Rahman, and A. Brahmi, "Adaptive force and position control based on quasi-time delay estimation of exoskeleton robot for rehabilitation," *IEEE Trans. Control Syst. Technol.*, vol. 28, no. 6, pp. 2152–2163, Nov. 2020.

[23] E. J. Park et al., "A hinge-free, non-restrictive, lightweight tethered exosuit for knee extension assistance during walking," *IEEE Trans. Med. Robot. Bionics*, vol. 2, no. 2, pp. 165–175, May 2020.

[24] Z. Taha et al., "A hybrid active force control of a lower limb exoskeleton for gait rehabilitation," *Biomedizinische Technik*, vol. 63, no. 4, pp. 491–500, 2018.

[25] M. Moltedo et al., "Variable stiffness ankle actuator for use in robotic-assisted walking: Control strategy and experimental characterization," *Mechanism Mach. Theory*, vol. 134, pp. 604–624, 2019.

[26] C. Siviy et al., "Offline assistance optimization of a soft exosuit for augmenting ankle power of stroke survivors during walking," *IEEE Robot. Automat. Lett.*, vol. 5, no. 2, pp. 828–835, Apr. 2020.

[27] V. H. Duenas, C. A. Cousin, A. Parikh, P. Freeborn, E. J. Fox, and W. E. Dixon, "Motorized and functional electrical stimulation induced cycling via switched repetitive learning control," *IEEE Trans. Control Syst. Technol.*, vol. 27, no. 4, pp. 1468–1479, Jul. 2019.

[28] C.-H. Chang and V. H. Duenas, "Switched motorized and functional electrical stimulation cycling controllers for power tracking," in *Proc. IEEE 58th Conf. Decis. Control*, 2019, pp. 1436–1441.

[29] M. Mahvash and P. E. Dupont, "Stiffness control of surgical continuum manipulators," *IEEE Trans. Robot.*, vol. 27, no. 2, pp. 334–345, Apr. 2011.

[30] X. Li, Y.-H. Liu, and H. Yu, "Iterative learning impedance control for rehabilitation robots driven by series elastic actuators," *Automatica*, vol. 90, pp. 1–7, 2018.

[31] J. Zhang and S. H. Collins, "The iterative learning gain that optimizes real-time torque tracking for ankle exoskeletons in human walking under gait variations," *Front. Neurorobot.*, vol. 15, 2021, Art. no. 653409.

[32] M. Norrlöf, "An adaptive approach to iterative learning control with experiments on an industrial robot," in *Proc. IEEE Eur. Control Conf.*, 2001, pp. 220–225.

[33] D. A. Bristow and A. G. Alleyne, "A manufacturing system for microscale robotic deposition," in *Proc. IEEE Amer. Control Conf.*, 2003, pp. 2620–2625.

[34] D. A. Bristow, M. Tharayil, and A. G. Alleyne, "A survey of iterative learning control," *IEEE Control Syst. Mag.*, vol. 26, no. 3, pp. 96–114, Jun. 2006.

[35] K. S. Lee and J. H. Lee, "Convergence of constrained model-based predictive control for batch processes," *IEEE Trans. Autom. Control*, vol. 45, no. 10, pp. 1928–1932, Oct. 2000.

[36] U. Rosolia and F. Borrelli, "Learning model predictive control for iterative tasks. A data-driven control framework," *IEEE Trans. Autom. Control*, vol. 63, no. 7, pp. 1883–1896, Jul. 2018.

[37] W. E. Dixon, E. Zergeroglu, D. M. Dawson, and B. T. Costic, "Repetitive learning control: A Lyapunov-based approach," *IEEE Trans. Syst., Man, Cybern., Part B*, vol. 32, no. 4, pp. 538–545, Aug. 2002.

[38] C.-H. Chang, J. Casas, and V. H. Duenas, "A switched systems approach for closed-loop control of a lower-limb cable-driven exoskeleton," in *Proc. IEEE Amer. Control Conf.*, 2022, pp. 4341–4346.

[39] S. Obuz, V. H. Duenas, R. J. Downey, J. R. Klotz, and W. E. Dixon, "Closed-loop neuromuscular electrical stimulation method provides robustness to unknown time-varying input delay in muscle dynamics," *IEEE Trans. Control Syst. Technol.*, vol. 28, no. 6, pp. 2482–2489, Nov. 2020.

[40] F. L. Lewis, D. M. Dawson, and C. T. Abdallah, *Robot Manipulator Control Theory and Practice*. New York, NY, USA: Marcel Dekker, 2004.

[41] M. Ferrarin and A. Pedotti, "The relationship between electrical stimulus and joint torque: A dynamic model," *IEEE Trans. Rehabil. Eng.*, vol. 8, no. 3, pp. 342–352, Sep. 2000.

[42] N. Sharma, K. Stegath, C. M. Gregory, and W. E. Dixon, "Nonlinear neuromuscular electrical stimulation tracking control of a human limb," *IEEE Trans. Neural Syst. Rehabil. Eng.*, vol. 17, no. 6, pp. 576–584, Dec. 2009.

[43] T. Schauer et al., "Online identification and nonlinear control of the electrically stimulated quadriceps muscle," *Control Eng. Pract.*, vol. 13, no. 9, pp. 1207–1219, 2005.
[44] M. J. Bellman, R. J. Downey, A. Parikh, and W. E. Dixon, "Automatic control of cycling induced by functional electrical stimulation with electric motor assistance," *IEEE Trans. Automat. Sci. Eng.*, vol. 14, no. 2, pp. 1225–1234, Apr. 2017.
[45] J. L. Krevolin, M. G. Pandy, and J. C. Pearce, "Moment arm of the patellar tendon in the human knee," *J. Biomech.*, vol. 37, no. 5, pp. 785–788, 2004.
[46] W. L. Buford et al., "Muscle balance at the knee - moment arms for the normal knee and the ACL-minus knee," *IEEE Trans. Rehabil. Eng.*, vol. 5, no. 4, pp. 367–379, Dec. 1997.
[47] H. K. Khalil and J. W. Grizzle, *Nonlinear Systems*. Upper Saddle River, NJ, USA: Prentice-Hall, 2002.
[48] A. Filippov, "Differential equations with discontinuous right-hand side," *Amer. Math. Soc. Transl.*, vol. 42, pp. 199–231, 1964.
[49] N. Fischer, R. Kamalapurkar, and W. E. Dixon, "LaSalle-Yoshizawa corollaries for nonsmooth systems," *IEEE Trans. Autom. Control*, vol. 58, no. 9, pp. 2333–2338, Sep. 2013.
[50] B. E. Paden and S. Sastry, "A calculus for computing Filippov's differential inclusion with application to the variable structure control of robot manipulators," *IEEE Trans. Circuits Syst.*, vol. 34, no. 1, pp. 73–82, Jan. 1987.
[51] C.-H. Chang, J. Casas, S. W. Brose, and V. H. Duenas, "Closed-loop torque and kinematic control of a hybrid lower-limb exoskeleton for treadmill walking," *Front. Robot. AI*, vol. 8, pp. 1–19, 2022.

CHEN-HAO CHANG received the Bachelor of Science degree in aeronautics and astronautics engineering from the National Cheng Kung University, Taiwan, in 2014, the Master of Science degree in aerospace engineering from the University of Florida, Gainesville, Fl, USA, in 2018, and the Ph.D. degree in mechanical engineering from Syracuse University, Syracuse, NY, USA, in 2022, under the supervision of Dr. Duenas. His research interests include nonlinear control theory, exoskeleton and cycling rehabilitation robotics, muscle stimulation, and delay control design.

JONATHAN CASAS received the B.Sc. and M.Sc. degrees in electrical engineering from the Colombian School of Engineering Julio Garavito, Bogota, Colombia, in 2016 and 2019, respectively. He is currently working toward the Ph.D. degree with the Bionics, Systems and Control Lab, Syracuse University, Syracuse, NY, USA, under the supervision of Dr. Victor Duenas. His research interests include data-driven adaptive control for switching systems, rehabilitation robotics, and human-robot interaction.

VICTOR H. DUENAS (Member, IEEE) received the Ph.D. degree from the Department of Mechanical and Aerospace Engineering, University of Florida, Gainesville, FL, USA, in 2018. In 2018, he joined the Department of Mechanical and Aerospace Engineering, Syracuse University, Syracuse, NY, USA, as an Assistant Professor. His research interests include nonlinear and adaptive control for rehabilitation robotics, neuromuscular control, and human-robot interaction.